Seismic Resilience Assessment of Geogrid-Encased Stone Column Composite Foundations

Xiaocong Cai[1-3,*]

[1]College of Civil Engineering, Hunan University, Changsha 410082, China

[2]Key Laboratory of Building Safety and Energy Efficiency of the Ministry of Education, Hunan University, Changsha 410082, China

[3]National Center for International Research Collaboration in Building Safety and Environment, Hunan University, Changsha 410082, China

Abstract: The post-earthquake functionality and rapid recovery of infrastructure built on soft soil depend critically on the resilience of geogrid-encased stone columns (GESCs) composite foundation systems. A coupled analytical and machine-learning framework is established to evaluate the seismic resilience of GESC composite foundations, aiming to identify key design parameters that govern earthquake recovery. The resulting damage states are translated into time-dependent functionality curves using a performance-based analytical approach. A comprehensive parametric study investigates the influence of different recovery functions, geogrid encasement strength, column diameter, spacing, area replacement ratio, layout configuration, and the internal friction angle of the column infill material on the functionality (Q) and resilience index (R). Results indicate that the Q is completely lost when k_h exceeds 0.75. When k_h exceeds 0.55, the system enters the low-resilience zone. The introduction of geogrid encasement significantly enhances both Q and R of OSC. Even at a high seismic intensity (k_h = 0.95), a GESC with 400 kN/m encasement strength retains a moderate resilience level. Resilience is maximized by a specific configuration: using high-friction materials to construct small-diameter columns with high encasement strength, arranged in a tight triangular pattern.

Keywords: Geogrid-Encased Stone Column, Seismic Resilience, Fragility Curve, Ultimate Seismic Bearing Capacity, Machine Learning.

1. INTRODUCTION

The escalating concentration of population and critical infrastructure in seismically active coastal and deltaic regions has brought the seismic performance of foundations on soft soil into sharp focus. Structures built on such vulnerable subsoils are not only subjected to amplified ground motions but also face catastrophic risks of bearing capacity failure, excessive settlement, and liquefaction-induced lateral spreading during earthquakes [1, 2]. The aftermath of major seismic events consistently reveals that the prolonged downtime and exorbitant economic losses are often attributable not merely to the collapse of superstructures, but to the pervasive and complex failure of their supporting foundations, which are notoriously difficult and time-consuming to repair [3, 4]. Consequently, modern seismic design for geotechnical engineering systems is shifting from a focus solely on life safety (collapse prevention) to one that prioritizes resilience [5, 6].

To mitigate the risks associated with weak soils, ground improvement techniques are indispensable. Among these, ordinary stone columns (OSCs) have been widely adopted to enhance bearing capacity, reduce settlement, and accelerate consolidation [7-12]. A significant advancement in this technology is the use of geogrid encasement, which confines the stone column, prevents bulging in very soft soils, and significantly improves its stiffness and load-carrying capacity [13-19]. Extensive research has validated the static performance of geogrid-encased stone columns (GESCs), focusing on their reinforcement mechanisms, load-settlement behavior, and design under vertical loads [20-25]. Most studies have begun to explore the dynamic response of GESC-reinforced ground, analyzing acceleration amplification, liquefaction potential mitigation, and permanent deformation under sinusoidal loading [26-29]. In the actual seismic loading, researchers [30-34] mainly used the shaking stable tests and numerical simulations to investigate the change in deformation, stress, and acceleration of GESC composite foundations.

Early and numerous studies have investigated the static performance and dynamic response (e.g., settlement, acceleration, and liquefaction potential) of OSCs/GESCs under both sinusoidal and earthquake loading. The field has progressively moved towards performance-based and reliability-focused approaches. Recent studies have developed fragility analyses for stone column systems, including assessments for OSCs [35, 36] and GESCs [37, 38]. These works address the critical need to quantify the failure probability under seismic excitation, considering

*Address correspondence to this author at the College of Civil Engineering, Hunan University, Changsha 410082, China; Key Laboratory of Building Safety and Energy Efficiency of the Ministry of Education, Hunan University, Changsha 410082, China and National Center for International Research Collaboration in Building Safety and Environment, Hunan University, Changsha 410082, China E-mail: xiaocongcai@hnu.edu.cn

Received on 05-05-2026 Accepted on 08-06-2026 Published on 09-06-2026

E-ISSN: 3083-3590/26

parameter uncertainties. Nevertheless, current seismic assessments of GECS predominantly focus on quantifying initial performance degradation or peak response during excitation, largely overlooking the post-event recovery phase. Geosynthetic materials can complicate the column-soil interaction and require special consideration in fragility and resilience assessments. True seismic resilience is a time-dependent metric that integrates both the depth of functionality loss and the speed of its restoration [39]. Moreover, there are few reports on the influence of key design parameters like encasement stiffness, column geometry, and layout on the post-earthquake recovery process and their quantified relationship. The existing design codes and studies lack a framework to optimize GESC systems not just for strength, but for rapid recoverability, which is paramount for lifeline infrastructure like transportation hubs and utility networks. Therefore, unlike conventional studies [26, 40] that focus solely on seismic resistance (e.g., bearing capacity and deformation), this study develops a time-variant resilience assessment framework for GESC composite foundations. This framework uniquely integrates the seismic fragility, post-earthquake functionality loss, repair duration, and recovery trajectory models into a unified workflow, ultimately yielding a quantifiable resilience index that includes both functionality loss and recovery speed.

This study proposes a comprehensive performance-based framework for the seismic resilience assessment of GESC composite foundations. In contrast to conventional force- or displacement-based methods, the proposed approach defines and quantifies functionality and resilience indices. These indices are designed to capture the system's integrated performance across the entire timeline, from the initial earthquake event through complete functional recovery. The ultimate seismic bearing capacity-based failure probability, damage state, economic and functional loss, repair time, and recovery function are incorporated into a neural network (NN) to analyze the functionality and seismic resilience of GESC composite foundations. Furthermore, a systematic parametric investigation into the effects of six critical design factors—geogrid stiffness, column diameter, spacing, area replacement ratio, arrangement pattern, and infill material shear strength—on both the immediate performance and the recovery process is conducted to provide practical and resilience-oriented design insights.

2. SEISMIC RESILIENCE ASSESSMENT FRAMEWORK

2.1. Seismic Bearing Capacity

The ultimate seismic bearing capacity (q_u) of the GESC composite foundation under a circular footing is expressed as:

$$q_u = 1.2cN_{cE} + q_1N_{qE} + 0.3\gamma BN_{\gamma E} \quad (1)$$

$$N_{qE} = \frac{P_{aq}\sin(\alpha_1+\alpha_2-\varphi_n-\varphi)}{q_1B[(1-k_v)sin(\alpha_2-\varphi_n)+k_h\cos(\alpha_2-\varphi_n)]} \quad (2)$$

$$N_{cE} = \frac{P_{ac}\sin(\alpha_1+\alpha_2-\varphi_n-\varphi)+c_n|ac|\cos(\varphi_n)-cr_0\,cos(\alpha_1+\alpha_2-\varphi_n)}{cB[(1-k_v)sin(\alpha_2-\varphi_n)+k_h\cos(\alpha_2-\varphi_n)]} \quad (3)$$

$$N_{\gamma E} = \frac{P_{a\gamma}\sin(\alpha_1+\alpha_2-\varphi_n-\varphi)-k_hW\cos(\alpha_2-\varphi_n)-(1-k_v)W\sin(\alpha_2-\varphi_n)}{0.5\gamma B^2(1-k_v)\sin(\alpha_2-\varphi_n)+k_hB\cos(\alpha_2-\varphi_n)} \quad (4)$$

where, N_{cE}, N_{qE}, and $N_{\gamma E}$ are seismic bearing capacity factors accounting for the inertial effects induced by seismic loading; $q_1 = \gamma_s h_0$ is the overburden pressure; h_0 is the embedded depth of foundation; B is the width of the footing; $k_h = \alpha_h/g$ and $k_v = \alpha_v/g$ are horizontal and vertical acceleration coefficients, respectively; α_h and α_v are the horizontal and vertical peak ground acceleration, respectively; g is gravitational acceleration; the angles (α_1~α_4) can be calculated based on Cai *et al*. [37]; c and φ are the cohesion and angle of internal friction of the GESCs composite foundation, respectively; c_n and φ_n are the reduced cohesion and angle of internal friction of the GESCs composite foundation, respectively; P_{aq}, P_{ac}, and $P_{a\gamma}$ are the forces on the *bc* side, contributed by q, c, and γ terms, respectively; r_0 is the length of the *bc* side; W is the weight of the composite foundation. Specific derivation and verification of q_u can refer to previous articles [37]. The composite properties of the GESC composite foundation are defined by weighted averaging as follows:

$$c = (1-m)c_s + m(c_c + c_g) \quad (5)$$

$$tan\varphi = (1-m)tan\varphi_s + mtan\varphi_c \quad (6)$$

$$\gamma = (1-m)\gamma_s + m\gamma_c \quad (7)$$

where, m is the area replacement ratio; c_g is apparent cohesion provided by geogrid encasement, which is related to the column diameter (D_c) and encasement strength (T); γ is the weight of the GESCs composite foundation; c_s, φ_s, and γ_s are the cohesion, angle of internal friction, and weight of the surrounding soil, respectively; c_c, φ_c, and γ_c are the cohesion, angle of internal friction, and weight of the column material, respectively.

2.2. Failure Probability

The ultimate bearing capacity (q_u) is a non-deterministic parameter whose evaluation requires multiple inputs. The assessment of seismic performance must be expressed probabilistically through fragility functions, which quantify the likelihood of failure under seismic excitation. Failure of the GESC composite foundation is defined as the condition where the vertical load demand (P_v) exceeds the ultimate

bearing capacity (q_u). Otherwise, the foundation is considered stable. The material weight of soil and stone aggregates is fixed as 17 kN/m^3 and 18 kN/m^3, respectively. The column materials with a φ_c range of 35°~45° (mean value of 40°) and c_c range of 5~20 kPa (mean value of 10 kPa) are used. The soil materials with a φ_s range of 15°~30° (mean value of 25°) and c_c range of 10~50 kPa (mean value of 15 kPa) are used. The mean value of T (range of 1~4 kN/m) and D_c (range of 0.04~0.12 m) are 2.5 kN/m and 0.08 m, respectively. The m with a range of 15%~35% and a mean m value of 25% is selected. Seven parameters with normal distribution for calculating q_u are used to analyze seismic failure probability (P_f). The neural network is used to analyze the seismic fragility of GESC composite foundations. The model is a feedforward neural network for binary classification. It has an input layer with 7 neurons (for the uncertain parameters of φ_c, φ_s, c_c, c_s, T, m, and D_c), two hidden layers with 64 and 32 neurons (using ReLU activation), and an output layer with 1 neuron (using a Sigmoid activation function to output the failure probability). The training dataset is generated via Monte Carlo simulation. For numerous random parameter combinations drawn from their statistical distributions, the corresponding ultimate bearing capacity is calculated using the analytical formulas. The network is trained using supervised learning to minimize the binary cross-entropy loss function. The probability estimates stabilized when the number of samples reached 10, 000, with a coefficient of variation below 0.05 [37]. The fragility curves produced by the neural network show excellent agreement with results from direct Monte Carlo simulation and logistic regression [37], confirming its accuracy. The loss and accuracy curves are presented in Figure **2**.

Specific verification and calculation can refer to previous research [37]. The definition of P_f at different damage states is presented in Table **2**. Figure **3** shows the failure probability of the GESC composite foundation at different states.

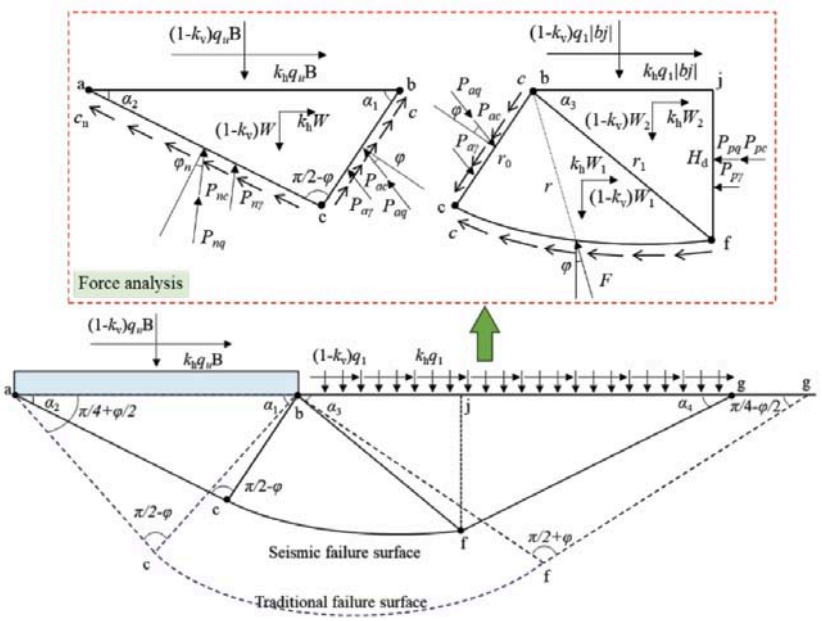

Figure 1: Force analysis and failure mode under seismic loading.

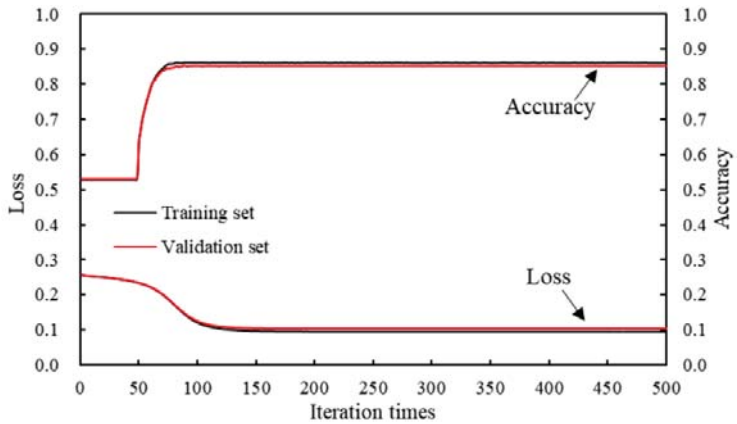

Figure 2: Loss and accuracy curves.

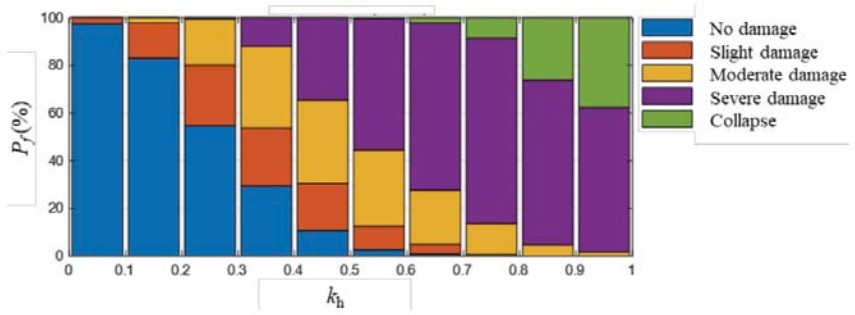

Figure 3: Failure probability of GESC composite foundation at different states.

2.3. Economic and Functional Loss

The direct economic losses (L) during earthquakes mainly consist of three components: main structure losses L_s, building decoration losses L_d, and indoor property losses L_c. The formula for calculating the direct economic loss (L) of a building during an earthquake can be expressed as [41]:

$$L = \alpha(L_s + L_d + L_c) \tag{8}$$

$$L_s = \sum_{i=1}^{n} \sum_{j=1}^{5} M_i P_j \mu_j^s \tag{9}$$

$$L_d = \gamma_1\gamma_2\gamma_3 \sum_{i=1}^{n} \sum_{j=1}^{5} \eta_1 M_i P_j \mu_j^d \tag{10}$$

$$L_c = \sum_{i=1}^{n} \sum_{j=1}^{5} \eta_2 M_i P_j \mu_j^c \tag{11}$$

where, $\alpha = 1.0$ is the seismic correction factor; M_i represents the reset cost; γ_1 = 1.15, γ_2 = 1.15, and γ_3 = 1.00 are the correction coefficients for decoration losses under different conditions, respectively; P_j is the failure probability in damaged state j; η_1 = 16% and η_2 = 0.5 are the decoration ratio and property ratio, respectively; μ_j^s, μ_j^d, and μ_j^c are the ratios of main structural loss, building decoration loss, and indoor property loss in the damaged state j, respectively.

The prototype column diameter and length are 0.4 m and 5 m, respectively. The columns are arranged in a square shape, and the column spacing is 1.0 m. The repair area is taken as 10 m × 10 m. The volume of 81 GESC is about 50.894 m^3, the soil volume of the treatment area is 449.106 m^3, and the geogrid area is about 508.938 m^3. The reset cost is calculated and summarized in Table **1**, and different loss ratios are presented in Table **2**.

When considering the overall condition of building structural damage, the functional loss ratio (L_k) is represented by the direct economic loss of the building, as follows:

$$L_k = L/M_i \tag{12}$$

Figure **4** shows the functional loss ratio of the GESC composite foundation under different k_h conditions. An increase in k_h results in a higher value of L L_k.

2.4. Repair Time

Structures will suffer certain degrees of damage after an earthquake and must be repaired to restore them to their pre-earthquake state as much as possible. The post-earthquake repair time is crucial. The following formula is given based on "Standard for Seismic Resilience Assessment of Buildings (GB/T 38591-2020)":

Table 1: Reset Cost Calculation Results

Material	Number	Price	M_i (yuan)
Stone aggregates	50.894 m^3	90 yuan/m^3	4580.460
Geogrid	508.938 m^2	2.0 yuan /m^2	1017.876
Foundation soil	449.106 m^3	45 yuan/m^3	20209.77

Table 2: Loss Ratio Values

Loss ratio	No damage	Slight damage	Moderate damage	Severe damage	Collapse
	>2.0P_v	1.5P_v ~2.0P_v	1.0P_v ~1.5P_v	0.4P_v ~1.0P_v	<0.4P_v
μ_j^s	0%	7%	20%	60%	100%
μ_j^d	0%	8%	20%	50%	90%
μ_j^c	0%	0%	5%	30%	80%

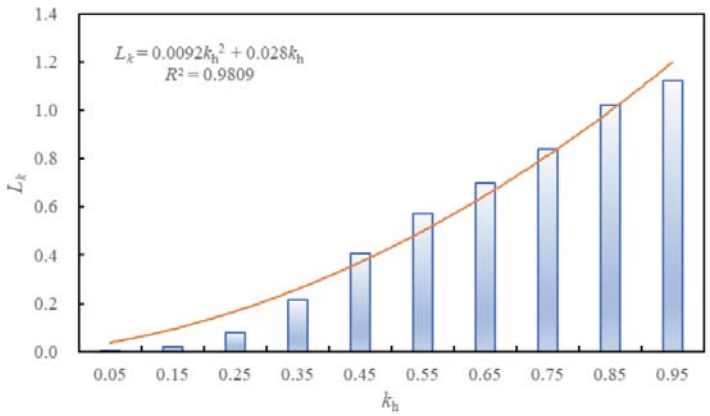

Figure 4: Functional loss ratio of GESC composite foundation under different k_h conditions.

$$T_{RE,W_i} = \frac{\sum_{i=1}^{m_{W_i}} Q_i}{N_{W_i}} \quad (13)$$

$$Q_i = \sum_{j=1}^{n} (Q_{(i,j)} \times n_{(i,j)}) \times \zeta_{T(i)} \times \lambda_T \quad (14)$$

$$N_{w_i} = q_{(r,w_i)} A = q_{(r,w_i)} n_{w_i} \quad (15)$$

Where, N_{w_i} is the number of workers required to complete a certain type of repair work (W_i); A is the repair area; n_{w_i} is the number of earthquake-damaged components included in the repair work (W_i); $q_{(r,w_i)}$ is the demand for the number of workers per unit area or single equipment; Q_i is the total repair time for the i-th type component; $Q_{(i,j)}$ is the repair time for the i-th type component in a damaged state j; $n_{(i,j)}$ is the number of i-th type components in a damaged state j; $\zeta_{T(i)}$ is the reduction factor for repair time considering the repair work quantity of the i-th type of earthquake-damaged component; λ_T = 1.0 is the influence parameter. Relative parameters (e.g., $n_{(i,j)}$ and $\zeta_{T(i)}$) can refer to the Post-earthquake field works-Part 4: Assessment for direct loss (GB/T 18208.4-2011). The final repair time is calculated and presented in Figure **5**.

2.5. Recovery Function

The process of restoring structural functionality is complex, influenced by the temporal and spatial dimensions. Therefore, different key facilities have different recovery paths, showing different recovery speeds and qualities. There is relatively little research on comprehensive models of the recovery process. In this study, linear, triangular, and exponential recovery functions [42] are selected for evaluating the seismic resilience of GESC composite foundations, as follows:

$$f_{rec}(t) = \begin{cases} 1, t < T_{OE} \\ a + b\frac{t-T_{OE}}{T_{RE}}, T_{OE} \le t \le T_{OE} + T_{RE} \text{(Linear function)} \\ a + b\left[1 - \cos\frac{\pi(t-T_{OE})}{2T_{RE}}\right], T_{OE} \le t \le T_{OE} + T_{RE} \text{(Triangular function)} \\ a\left[\exp\left(-b\frac{t-T_{OE}}{T_{RE}}\right)\right], T_{OE} \le t \le T_{OE} + T_{RE} \text{(Exponential function)} \\ 1, t > T_{OE} + T_{RE} \end{cases} \quad (16)$$

where, $f_{rec}(t)$ is the recovery function; t is the repair time; T_{OE} is the time of earthquake occurrence; T_{RE} is the post-earthquake repair time; a and b are correlation coefficients.

3. RESULTS AND DISCUSSIONS

The parameters from Sections 2.4~2.6 depend on regional or project-specific conditions; therefore, localized calibration is recommended in practical applications. To ensure complete structural repair, the resilience assessment time T_{total} and T_{OE} are taken as

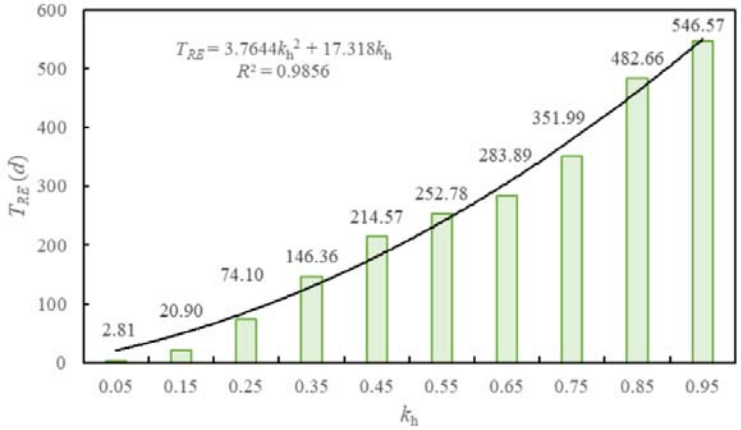

Figure 5: Repair time of GESC composite foundation under different k_h conditions.

550 *d* and 0 *d*, respectively. The correlation coefficients (i.e., *a* and *b*) can be derived based on the boundary conditions (i.e., $f_{rec}(0) = 1 - L_k$ and $f_{rec}(T_{OE} + T_{RE}) = 1$). Therefore, for both linear and triangular recovery functions, the parameters are derived as $a = 1 - L_k$ and $b = L_k$. For the exponential recovery function, the parameters are derived as $a = 1 - L_k$ and $b = \ln^{(1 - Lk)}$. By incorporating the recovery function, the complete functionality recovery function ($Q(t)$) can be obtained, as follows:

$$Q(t) = \begin{cases} 1, t < T_{OE} \\ f_{rec}(t), T_{OE} \le t \le T_{OE} + T_{RE} \\ 1, t > T_{OE} + T_{RE} \end{cases} \quad (16)$$

Figure **6a**, **b**, and **c** present the change in the functionality of GESC composite foundations over time under different seismic intensities, respectively, for linear, triangular, and exponential recovery functions. The linear model assumes a constant rate of recovery following the cessation of earthquake ground motion. In Figure **6a**, structural repair efforts proceed at a uniform pace, suggesting an idealized situation with consistent resource allocation and labor availability. GESC composite foundations exhibit rapid and efficient recovery under low-to-moderate intensity (e.g., $k_h \le 0.45$), reaching full functionality ($Q = 1.0$) well before the 215-day. The triangular model in Figure **6b** introduces a pronounced time lag or "pre-repair" phase before the onset of significant functional gain. This non-linear behavior is characteristic of scenarios involving complex decision-making, logistical bottlenecks, or the need for extensive safety inspections prior to initiating repairs. The exponential model in Figure **6c** demonstrates a rapid recovery phase. As k_h increases, indicating greater structural damage and longer repair time, the functionality of GESC composite foundations significantly reduces. Notably, for high-intensity scenarios (e.g., $k_h > 0.75$), the recovery process is significantly prolonged, with the system struggling to regain full operational capacity within the defined timeframe. The complete loss of functionality is observed when k_h exceeds 0.75.

Resilience index (R) is defined as the ratio of the shaded area below the functional recovery function to the repair time, as shown in Figure **7**. The calculation formula is as follows:

$$R = \int_{T_{OE}}^{T_{total}} Q(t)/(T_{total} - T_{OE})dt \quad (17)$$

$$R(t, k_h) = \frac{1}{t}\int_0^t Q(t, k_h)\, dt \quad (18)$$

When R = 0.90~1.00, it is considered that the structural component is at a normal resilience level. When R = 0.85~0.90, it is considered that the structural component is at a moderate resilience level. When R is below 0.85, it is considered to be at a low resilience level. The selection of the resilience index threshold refers to the previous studies [43, 44].

Figure **8a** shows the different resilience curves of the GESC composite foundation under different k_h values. The resilience index is significantly negatively

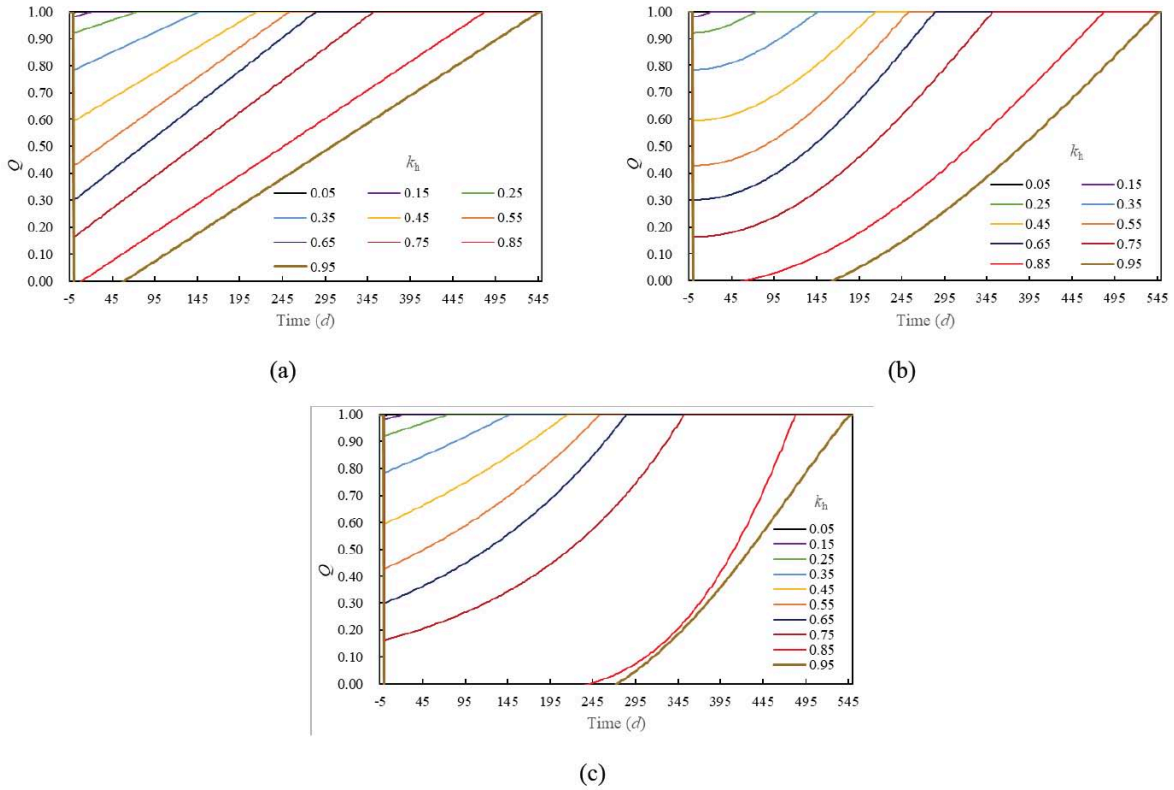

Figure 6: Functional recovery curve under different seismic intensities: (**a**) linear type; (**b**) triangle type; (**c**) exponential type.

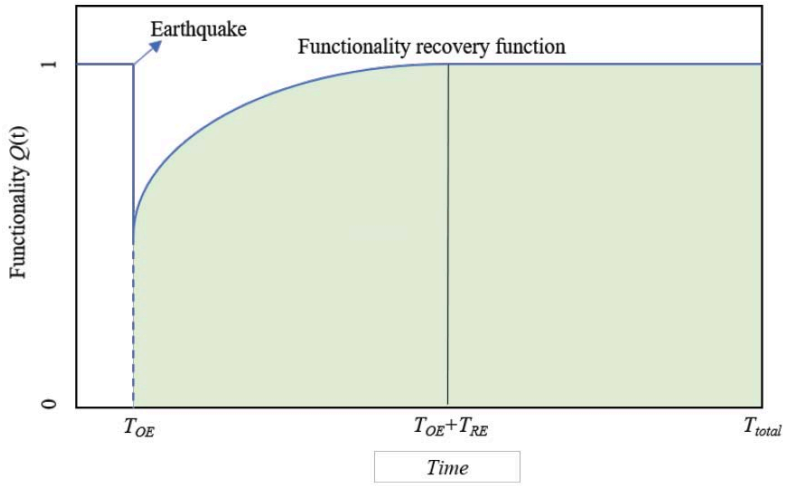

Figure 7: Functionality recovery function and definition of resilience.

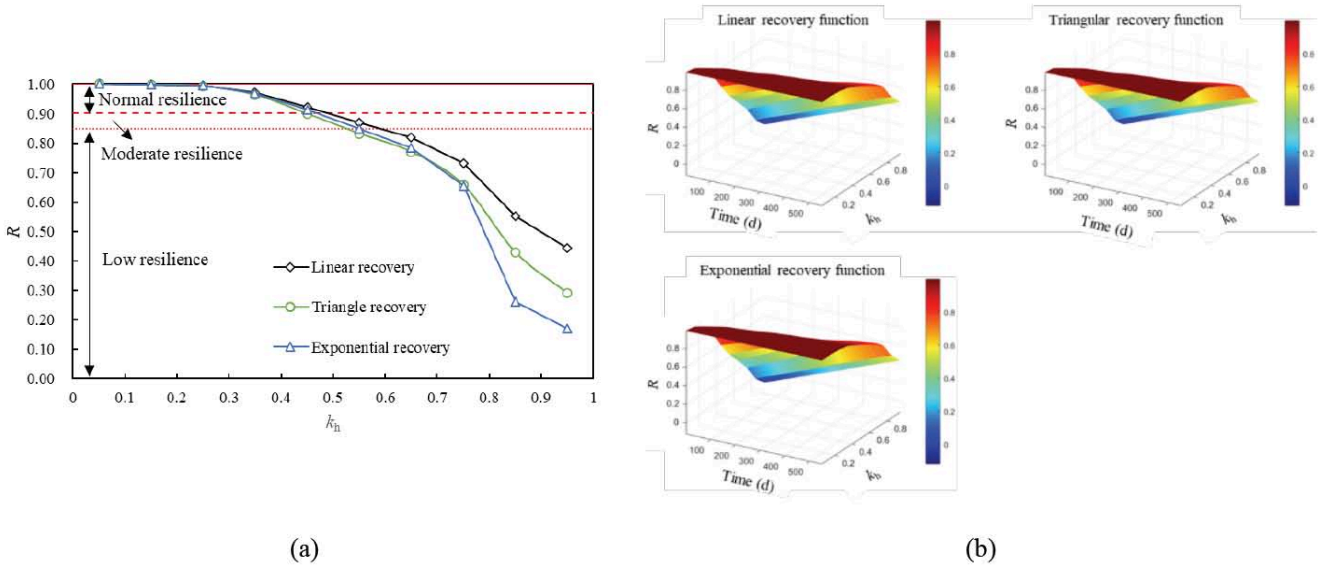

Figure 8: Resilience calculation results: (**a**) resilience curve and (**b**) resilience surface.

correlated with the peak ground acceleration. When $k_h \leq 0.45$, the resilience index remains above the normal level threshold ($1.00 \geq R \geq 0.90$). When $0.55 \geq k_h > 0.45$, the resilience index enters the moderate level range ($0.90 > R \geq 0.85$). When $k_h > 0.55$, the resilience index has decayed to below the low resilience level ($R < 0.85$), indicating that the increase in seismic intensity leads to a fundamental deterioration of the structural seismic resilience. Figure **8b** shows the different resilience surfaces of the GESC composite foundation under different k_h values and repair times. Repair times have a remarkable influence on the R values. Under strong earthquake action, even after repair, the GESC composite foundation may still be at a moderate or even low resilience level. To enhance the functional recoverability and resilience of systems under earthquake, it is necessary to establish a multi-index resilience evaluation system, such as optimizing the encasement strength, column diameter, and spacing.

4. RESILIENCE ENHANCEMENT STRATEGY

4.1. Effect of Encasement Strength

The exponential recovery model is used for investigating the effect of different parameters on the functionality and resilience of GESC composite foundations. Figure **9a** illustrates the functionality of GESC composite foundations with different encasement strengths (T) over time under a moderate seismic intensity. While the ordinary stone columns (OSCs) exhibit more serious damage and slower recovery, the introduction of geogrid encasement initiates a significant shift (e.g., T = 0 and 50 kN/m). Systems with higher T values demonstrate accelerated recovery rates. Figure **9b** evaluates the resilience index (R) as a function of seismic intensity for varying T. R increases with increasing T. Conversely, under severe seismic excitations, the OSC exhibits catastrophic resilience collapse. The difference in R

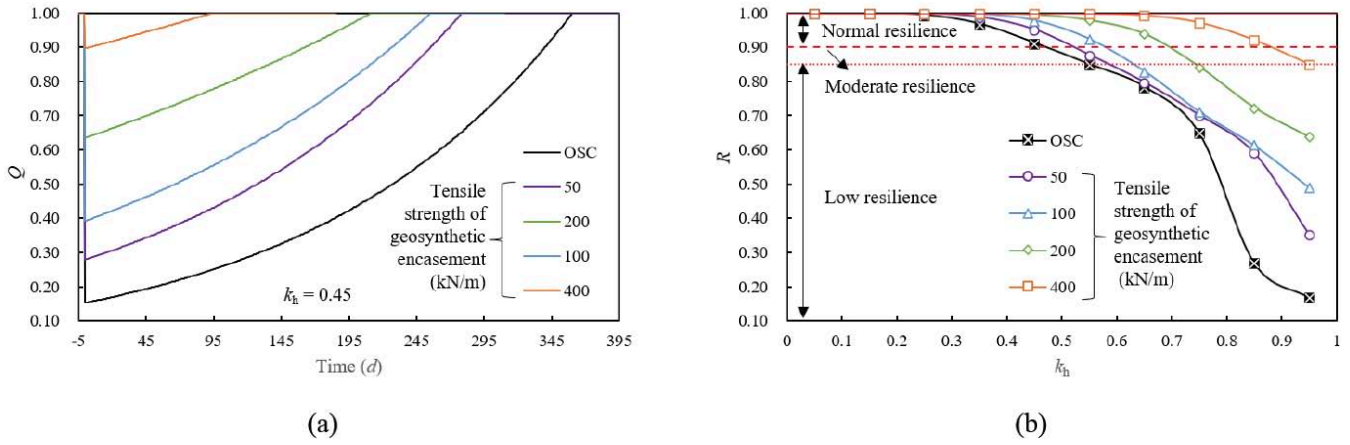

Figure 9: Effect of encasement strength on: (**a**) *Q* and (**b**) *R*.

between OSC and GESC with *T* of 50~100 kN/m is relatively small at k_h = 0~7.5. As k_h exceeds 0.55, the resilience of the OSC system significantly decreases and enters the low resilience zone. GESC systems retain substantial resilience. Even at k_h = 0.95, the GESC with encasement strength of 400 kN/m sustains an *R* value of approximately 0.85 (i.e., moderate resilience).

Increasing encasement strength provides higher confining stress, preventing the total system breakdown observed in OSC and ensuring operational continuity. While high strength alone cannot prevent the initial damage caused by high k_h, it critically dictates the speed and completeness of the subsequent recovery. High-strength reinforcement can more effectively limit the bulging deformation of stone columns under horizontal and vertical seismic forces, directly increasing the equivalent cohesion and stiffness of the column. Therefore, GESC can withstand higher shear stresses during earthquakes, thereby reducing irreversible plastic deformation and settlement (i.e., lower initial functional loss). For critical infrastructure in high-seismic-risk areas, high-strength reinforced materials fundamentally prevent the system from entering a state of severe damage, thereby ensuring repair feasibility and speed.

4.2. Effect of Column Diameter

Figure **10a** and **b** present a comprehensive analysis of the influence of column diameter (D_c) on the *Q* and *R*, respectively. The data reveal a pronounced geometric sensitivity of the recovery process, demonstrating that structural dimensions significantly alter both *Q* and *R*. A clear negative correlation between D_c and *Q* is observed. A larger diameter delays the mobilization of encasement confinement, which is important for the performance of stone columns, significantly increasing the probability of structural damage. Therefore, the 1200 mm column achieves full functionality most slowly, with the recovery curve displaying the longest plateau duration. Similarly, a negative correlation between D_c and *R* is observed. The variation in *R* across different D_c values is relatively small, particularly when k_h is less than 0.75. Furthermore, a small-diameter column with relatively low bending stiffness can facilitate its adaptation to foundation deformation through minor bending and prevent excessive stress concentration. From a resilience perspective, using numerous densely

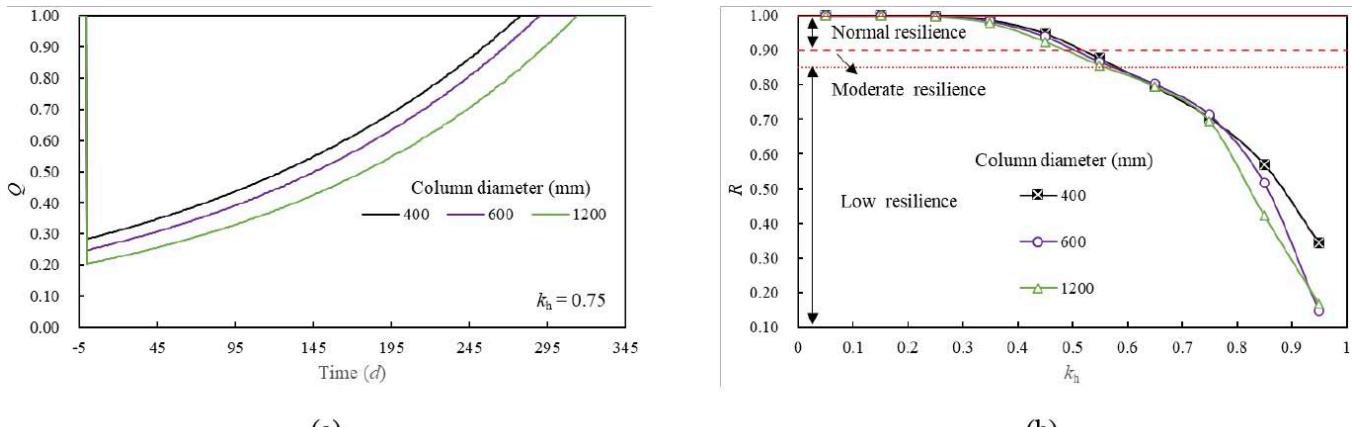

Figure 10: Effect of column diameter on: (**a**) *Q* and (**b**) *R*.

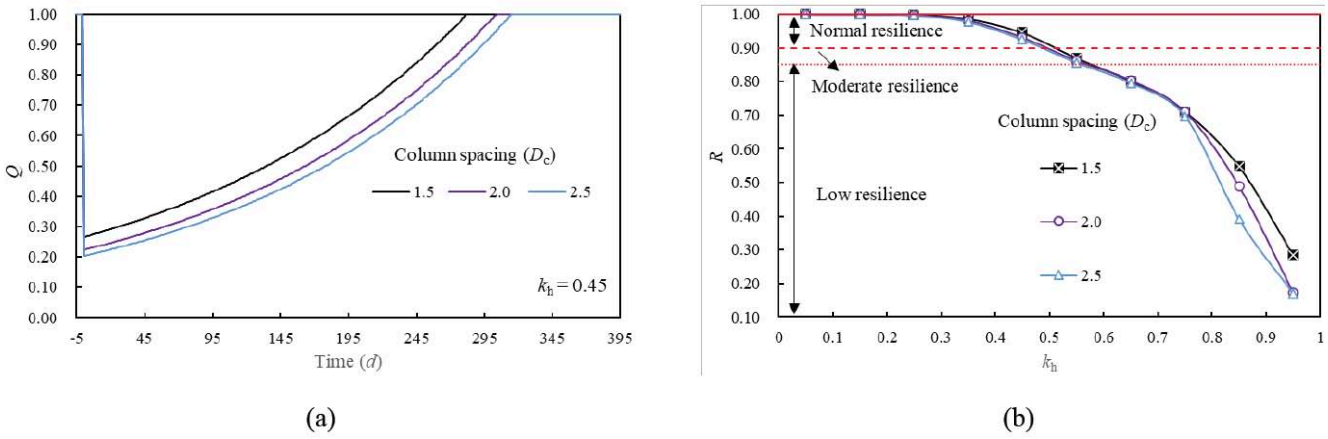

Figure 11: Effect of column spacing on: (**a**) *Q* and (**b**) *R*.

spaced small-diameter columns is often superior to a few sparsely spaced large-diameter columns.

4.3. Effect of Column Spacing

Figure **11a** illustrates the functional recovery curves for different column spacing (s = 1.5D_c, 2.0D_c, 2.5D_c) under k_h = 0.45. Specifically, the narrowest spacing (1.5D_c) achieves full functionality (Q=1.0) in approximately 282 days. In contrast, the widest spacing (2.5D_c) requires over 302 days to reach the same state. This time-displacement of approximately 7.1% suggests that wider column spacings degrade the system's operational efficiency during the recovery phase. As spacing increases, the tributary area served by each individual column expands, reducing the overall stiffness. Consequently, the superstructure experiences larger displacement demands and slower stabilization, even when subjected to the same intensity of seismic excitation. Figure **11b** plots the variation of *R* against seismic intensity, revealing a critical inverse relationship between column spacing and *R*. Under k_h < 0.75, the impact of different spacing configurations on *R* is minimal. However, as seismic intensity escalates into the severe range (k_h > 0.75), the sensitivity of the *R* to spacing becomes pronounced. The column spacing has a significant effect on the functionality and resilience of GESC composite foundations when the earthquake intensity is high. Under low-to-moderate seismicity (k_h < 0.5), all spacing configurations maintain normal resilience (*R* > 0.9). For k_h = 0.5~0.55, all spacing configurations maintain moderate resilience (0.9 > *R* > 0.85).

4.4. Effect of Area Replacement Ratio

Figure **12a** illustrates the time-dependent recovery of functionality for different area replacement ratios (*m* = 5%, 10%, and 30%). A critical observation is the positive relationship between *m* and *Q*. The configuration with *m* of 5% exhibits the lowest immediate functionality (dropping to approximately 0.18 immediately after the event), whereas the highest ratio (*m* = 30%) retains the highest initial capacity (around 0.25). This initial disadvantage associated with higher *m* likely stems from the stiffness increase introduced by the column. Figure **12b** plots the effect of area replacement ratio on *R* under different seismic intensities. An inverse relationship between *m* and *R* is obtained. In the low seismic intensities (k_h < 0.45), all configurations maintain normal resilience, suggesting that minor strengthening is adequate for typical seismic events. Moreover, the difference in *R* for different *m* is relatively small under k_h < 0.75. However, as the

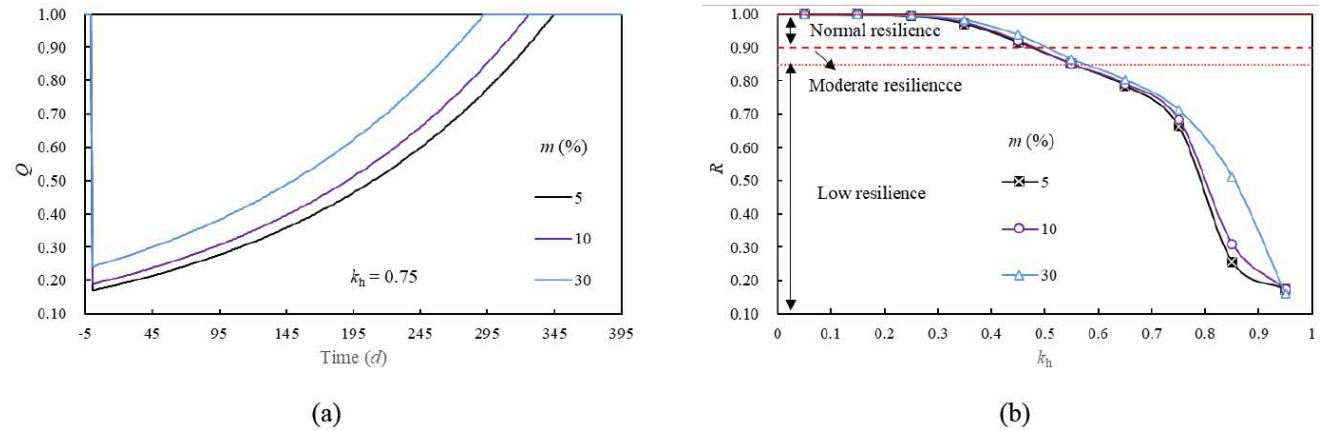

Figure 12: Effect of area replacement ratio on: (**a**) *Q* and (**b**) *R*.

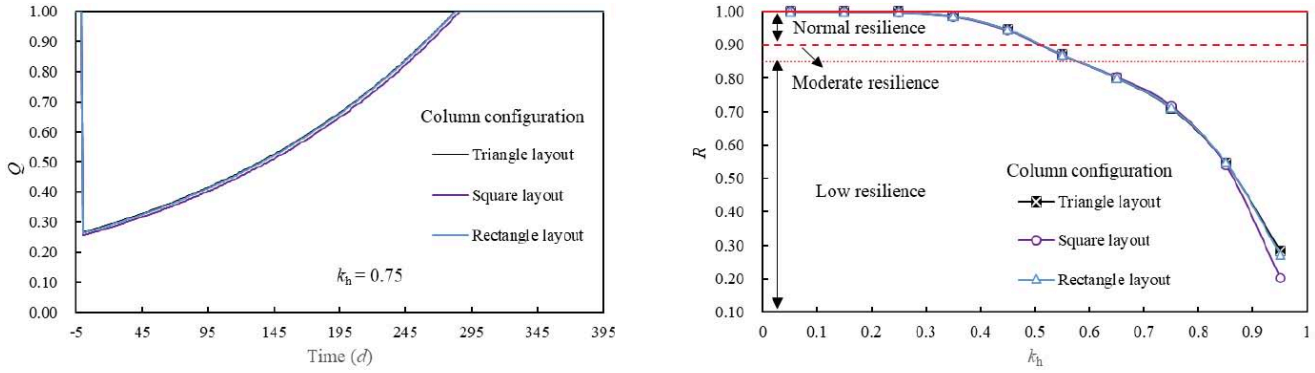

Figure 13: Effect of column configuration on: (**a**) *Q* and (**b**) *R*.

seismic intensity escalates beyond k_h = 0.75, a divergence in resilience capacity becomes pronounced. A high replacement ratio (*m* = 30%) provides substantial lateral confinement to the inner core, resulting in a more stable recovery process. Close spacing and high area displacement rate both indicate stronger column-soil-column interactions, which more effectively distribute loads from the superstructure and confine lateral movement in the soft soil layer. During earthquakes, this significantly reduces differential settlement and foundation rotation, thereby protecting the superstructure.

4.5. Effect of Column Configuration

Figure **13a** and **b** present the effect of column configurations on *Q* and *R*, respectively. The column configurations can be ranked in order of effectiveness from most to least effective as follows: triangular layout, rectangular layout, and square layout. The superior performance of the triangular layout can be mechanistically attributed to stress diffusion efficiency and geometric redundancy. Triangular grids, being the most efficient shape for resisting lateral loads in structural mechanics, facilitate a more uniform distribution of inelastic deformation. However, the influence of column configurations on both *Q* and *R* is also minimal.

4.6. Effect of Internal Friction Angle

Figure **14a** and **b** present the effect of internal friction angle (φ_c) of column material on *Q* and *R*, respectively. The functional recovery curves and resilience value demonstrate a clear positive correlation. Under lateral seismic forces, the column is subjected to significant bending and shear stresses. A higher internal friction angle enhances the inter-particle locking effect, providing greater shear strength. This prevents the phenomenon of column bulging or lateral squeezing, which is a primary cause of differential settlement in soft ground improvement. The system founded in dense stone (φ_c = 50°) exhibits the most rapid restoration of functionality, achieving full serviceability in approximately 317 days. In contrast, the loose stone configuration (φ_c = 35°) requires nearly 331 days to reach the same *Q*-value. A higher friction angle corresponds to a denser, more rigid granular skeleton. The superior recovery of the high-friction-angle piles indicates their superior capacity to withstand dynamic loading. Granular materials derive their strength primarily from friction. A column with φ_c of 50° dissipates significantly more energy through grain rearrangement and frictional sliding compared to a loose column (φ_c = 35°). The entire resilience profile shifts upwards with increasing

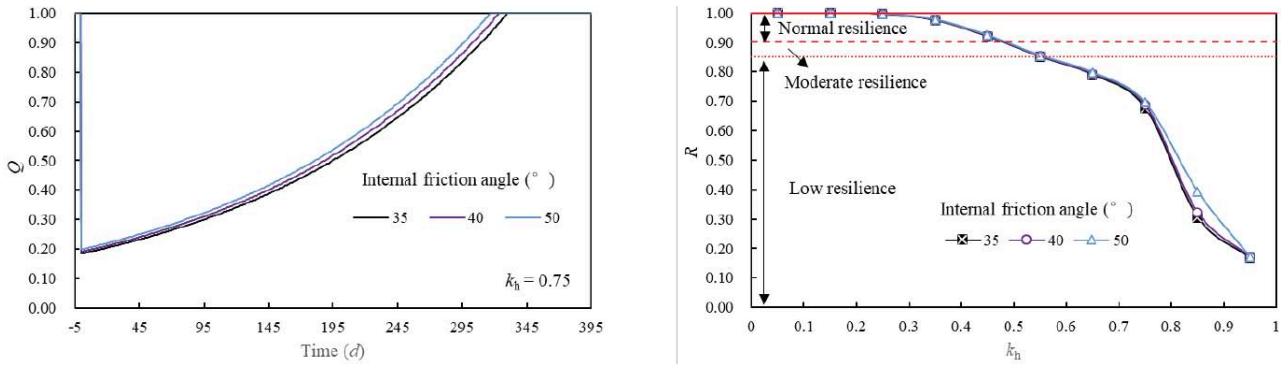

Figure 14: Effect of internal friction angle on: (**a**) *Q* and (**b**) *R*.

friction angle, signifying a reduction in the system's fragility to extreme seismic events. Reduced friction angles diminish the bearing capacity of the column, leading to larger permanent settlements and increased bending moments. However, the difference in R for different φ_c is relatively small under $k_h < 0.75$.

Based on the resilience assessment, a representative seismic intensity level (i.e., $k_h = 0.55$) is selected to compare the importance of each parameter. The range of parameters (i.e., encasement strength, column diameter, column spacing, area replacement ratio, column configuration, and internal friction angle) is typically used in the field. The enhancement of encasement strength provides the most significant improvement to R. A high T fundamentally increases the confining pressure, limiting initial damage depth and accelerating recovery. The effects of column diameter, column spacing, and area replacement ratio are moderate. The effect of column configuration and internal friction angle on the R is minor. While T is crucial for limiting the depth of loss, the geometric parameters (column diameter, column spacing, and area replacement ratio) are key to accelerating the recovery rate.

5. CONCLUSIONS

A calculation framework is developed for seismic resilience assessment of geogrid-encased stone columns (GESCs) composite foundations. The main conclusions are summarized as follows:

(1) The ultimate seismic bearing capacity (q_u) is calculated and used to evaluate the seismic fragility of GESC composite foundations. The failure probability, damage state, economic and functional loss, repair time, and recovery function are incorporated into a neural network (NN) to analyze the functionality and seismic resilience of GESC composite foundations.

(2) The functionality of GESC composite foundations is completely lost when k_h exceeds 0.75. The linear model has a rapid and efficient recovery in the initial stage, while the triangle and exponential models exhibit a pronounced time lag. An increase in k_h results in greater functional losses, longer repair times, and lower seismic resilience. When k_h exceeds 0.55, the resilience index drops below the low-resilience threshold.

(3) OSCs exhibit more severe damage and slower recovery, whereas the introduction of geogrid encasement initiates a marked improvement in resilience. Despite the extreme seismic intensity ($k_h = 0.95$), a GESC with 400 kN/m encasement strength retains a moderate resilience level. The most advantageous configuration for seismic resilience entails using high-friction materials to form small-diameter columns with high encasement strength, deployed in a tight triangular arrangement.

(4) The proposed resilience assessment framework provides a theoretical foundation and practical approach for shifting the design focus of critical infrastructure on soft soils from strength-based to resilience-based control. The optimal configuration identified in this study (high intensity, small diameter, densely spaced columns) may increase initial construction costs, but avoid the low resilience risks. The framework supports future code revisions and lifecycle cost-benefit analyses.

CREDIT AUTHORSHIP CONTRIBUTION STATEMENT

Xiaocong Cai: Methodology; Investigation; Writing - Original Draft; Data curation; Formal analysis; Conceptualization; Validation; Writing - Review & Editing.

DECLARATION OF COMPETING INTEREST

The authors declare that they have no known competing financial interests or personal relationships that could have appeared to influence the work reported in this paper.

DATA AVAILABILITY

Data will be made available on request.

REFERENCES

[1] Xiao S, Zhou G, Feng P, Qu Z. Seismic performance evaluation of novel RC frame structure with kinked rebar beams and post-yield hardening columns through shaking table tests. Eng Struct 2023; 290: 116375. https://doi.org/10.1016/j.engstruct.2023.116375

[2] Yan X-Y, Cao S-S, Zhao Z. Shaking Tables Test on Seismic Responses of a Long-Span Rigid-Framed Bridge Considering Traveling Wave Effect and Soil–Structure Interaction. Buildings 2024; 14(5): 1432. https://doi.org/10.3390/buildings14051432

[3] Eze KN, Anosike CU, Eze FN, Enabulele EC, Benson KP. Climate Resilient and Sustainable Infrastructures: Geotechnical Challenges of Problematic Soils in Nigeria. Civil and Environmental Engineering Reports 2024; 34(4): 521-538. https://doi.org/10.59440/ceer/195899

[4] Lee M, Basu D. An Integrated Approach for Resilience and Sustainability in Geotechnical Engineering. Indian Geotech J 2018; 48(2): 207-234. https://doi.org/10.1007/s40098-018-0297-3

[5] Hasheminezhad A, Ceylan H, Kim S, Tutumluer E. Geosynthetics for resilient geotechnics: A review of applications and innovations. Transp Geotech 2025; 55: 101676. https://doi.org/10.1016/j.trgeo.2025.101676

[6] Reddy KR, Janga JK, Kumar G. Sustainability and Resilience: A New Paradigm in Geotechnical and Geoenvironmental Engineering. Indian Geotech J 2025; 55(4): 2510-2531. https://doi.org/10.1007/s40098-024-00899-5

[7] Hosseinpour, I. Three-Dimensional Numerical Analysis of Embankment Overlying Geotextile-Encased Columns with Granular Platform. Iranian Journal of Science and Technology Transactions of Civil Engineering 2024; 48(3): 1641-1653. https://doi.org/10.1007/s40996-024-01390-0

[8] Ji M, Wang J, Zhao Y, Deng J, Zheng Y. Numerical Simulation of the Load Transfer Mechanism of a Geosynthetic Encased Stone Column Unit Cell under Embankment Loading. Int J Geomech 2024a; 24(8): 04024162. https://doi.org/10.1061/IJGNAI.GMENG-9393

[9] Liu K, Qiu R, Zhou P, Wang T, Connolly PD, Xiao J. Geotextile-encased cinder gravel columns: a coupled DEM-FDM analysis. Geosynth Int 2024; 1-44. https://doi.org/10.1680/jgein.23.00161

[10] Kang B-W, Wang J-Q, Zhou Y-W, Lin Z-N. Experimental analysis of compression bearing characteristics of multi-layer geogrid-encased aggregate column based on digital image measurement technology. Constr Build Mater 2024; 417: 135292. https://doi.org/10.1016/j.conbuildmat.2024.135292

[11] Krishnamurthy P, Maniam Rajan P. Comparative Study on the Reinforced Sand-Bed and the Stone Column in Improving the Clay Deposit Supporting Isolated Footing. Adv Civ Eng 2024; 2024(1): 8836116. https://doi.org/10.1155/2024/8836116

[12] Menon AR, Bhasi A. Evaluation of Critical Length of Encasement for Stone Column-Supported Embankment with Basal Geocell. Arabian J Sci Eng 2024; 49: 13821-13843. https://doi.org/10.1007/s13369-024-08778-0

[13] Castro Gonzalez J, Miranda Manzanares M, Justo Urrutia J. An analytical solution for the settlement of encased stone columns beneath rigid footings. Geotext Geomembr 2024; 52(4): 451-464. https://doi.org/10.1016/j.geotexmem.2024.01.001

[14] Elwakeel AO, Elsherbini RM. Effect of Column Material Internal Angle of Friction and the Geotextile Stiffness on the Behavior of Group of Geosynthetic-Encased Stone Column. Indian Geotech J 2024. https://doi.org/10.1007/s40098-024-01005-5

[15] Modalavalasa U, Ramanathan A. Performance of Encased Stone Column Aggregates Using Large-Scale Triaxial Testing. Geo-Congress 2024.

[16] Mohamed MK, Sakr MA, Azzam WR. Geotechnical behavior of encased stone columns in soft clay soil. Innovative Infrastruct Solutions 2023; 8(2): 80. https://doi.org/10.1007/s41062-023-01044-6

[17] Pandey Balbir K, Rajesh S, Chandra S. Electrokinetics in a Stone Column Encased by a Conductive Jute Geotextile: The Role of Anode Materials. Int J Geomech 2024; 24(6): 04024095. https://doi.org/10.1061/IJGNAI.GMENG-9545

[18] Qin XZ, Chen JF, He PC. Numerical simulation of bending characteristics of geosynthetic encased stone column. IOP Conf Ser Earth Environ Sci 2024; 1335(1): 012018. https://doi.org/10.1088/1755-1315/1335/1/012018

[19] Zeini HA, Lwti NK, Imran H, Henedy SN, Bernardo LFA, Al-Khafaji Z. Prediction of the bearing capacity of composite grounds made of geogrid-reinforced sand over encased stone columns floating in soft soil using a White-box machine learning model. Applied Sciences 2023; 13(8): 5131. https://doi.org/10.3390/app13085131

[20] Gu M, Cai X, Lu Y, Han D. Numerical investigation of cyclic load effects on geogrid-encased stone columns using a 3D coupled method. Soil Dyn Earthquake Eng 2025a; 193: 109332. https://doi.org/10.1016/j.soildyn.2025.109332

[21] Gu M, Cai X, Qiu J, Zhang X, Han D. Dynamic Behavior of Stone Column–Improved Soft Clay under Three-Stage Traffic Loads. Int J Geomech 2025b; 25(1): 04024322. https://doi.org/10.1061/IJGNAI.GMENG-10410

[22] Kumar N, Kumar R. Performance of Geosynthetic-Encased Stone Columns in Sandy Soils Subjected to Vertical Cyclic Loads. Int J Geomech 2025; 25(1): 04024323. https://doi.org/10.1061/IJGNAI.GMENG-10283

[23] Yoosefi S, Meehan CL, Garakani AA, Mosalmanzadeh A. Bearing Capacity of a Stone Column Constructed Using the Vibro-Replacement Method: Experimental and Numerical Investigations. Geo-Congress 2024.

[24] Yousuf S, Samadhiya NK. Numerical Evaluation of Pile Length, Lateral Bulging and Encasement Length: A Comparative Study on Ordinary and Encased Granular Piles. Int J Geosynth Ground Eng 2024; 10(3): 48. https://doi.org/10.1007/s40891-024-00556-0

[25] Zhang L, Peng B, Zhou S, Cui P, Liu Y. Numerical study on stability of geosynthetic-encased stone column-supported embankments based on equivalent method. Comput Geotech 2024; 169: 106179. https://doi.org/10.1016/j.compgeo.2024.106179

[26] Cai X, Zhang L, Yang Z, Mao B. Dynamic Behavior of GESC Groups in Sand Under Sinusoidal Loading: A Continuum-Discrete Coupled Analysis. Int J Numer Anal Methods Geomech 2025; 49(11): 2655-2669. https://doi.org/10.1002/nag.4000

[27] Ji M, Zhao Y, Li F, Zheng Y. Shaking table tests on the influence of geosynthetic encasement stiffness on the shear reinforcement effect of GESC composite foundation. Geotext Geomembr 2024b; 52(2): 209-220. https://doi.org/10.1016/j.geotexmem.2023.10.005

[28] Lakkimsetti B, Latha GM. Physico-mechanical aspects of liquefaction risk reduction in sand using geotextile-encased granular columns. Acta Geotech 2024; 19(10): 6843-6864. https://doi.org/10.1007/s11440-024-02402-z

[29] Zhang L, Cai X, Yang Z. Dynamic Response of GESCs-Supported Embankments in Sand Under Sinusoidal Loading: A Fluid-Solid Coupling Method. Int J Numer Anal Methods Geomech 2025; 49(16): 4001-4019. https://doi.org/10.1002/nag.70055

[30] Cengiz C, Guler E. Seismic behavior of geosynthetic encased columns and ordinary stone columns. Geotext Geomembr 2018a; 46(1): 40-51. https://doi.org/10.1016/j.geotexmem.2017.10.001

[31] Cengiz C, Guler E. Shaking table tests on geosynthetic encased columns in soft clay. Geotext Geomembr 2018b; 46(6): 748-758. https://doi.org/10.1016/j.geotexmem.2018.07.009

[32] Cengiz C, Guler E. Load bearing and settlement characteristics of Geosynthetic Encased Columns under seismic loads. Soil Dyn Earthquake Eng 2020; 136: 106244. https://doi.org/10.1016/j.soildyn.2020.106244

[33] Geng L, Tang L, Cong SY, Ling XZ, Lu J. Three-dimensional analysis of geosynthetic-encased granular columns for liquefaction mitigation. Geosynth Int 2017; 24(1): 45-59. https://doi.org/10.1680/jgein.16.00014

[34] Tang L, Cong S, Ling X, Lu J, Elgamal A. Numerical study on ground improvement for liquefaction mitigation using stone columns encased with geosynthetics. Geotext Geomembr 2015; 43(2): 190-195. https://doi.org/10.1016/j.geotexmem.2014.11.011

[35] Jasim OH, Khaleel F, Khaleel D, Fattah MY, Alfahad AA, AbdUlameer AH, Afan H. Predicting the factor of safety in embankments improved by geogrid-encased stone columns using various neural network architectures. Model Earth Syst Environ 2025; 11(6): 438. https://doi.org/10.1007/s40808-025-02635-1

[36] Qiu Z, Ebeido A, Prabhakaran A, Elgamal A, Zheng Y. Carbon Footprint and Seismic Fragility Assessment of a Bridge–Foundation–Ground System Using Stone Columns as Liquefaction Countermeasures. J Geotech Geoenviron Eng 2025b; 151(3): 04025005. https://doi.org/10.1061/JGGEFK.GTENG-12786

[37] Cai X, Zhang L, Yang Z, Tan J, Yue S. Seismic bearing capacity and fragility analysis of geogrid-encased stone column composite foundations. Geotext Geomembr 2026; 54(1): 99-114. https://doi.org/10.1016/j.geotexmem.2025.09.003

[38] Qiu R, Gou J, Liu K, El Naggar MH, Xiao K, Zheng L, Wang T. Seismic fragility analysis of geosynthetic-encased stone column composite foundation. Soil Dyn Earthquake Eng 2025a; 189: 109095. https://doi.org/10.1016/j.soildyn.2024.109095

[39] Bruneau M, Chang SE, Eguchi RT, Lee GC, O'Rourke TD, Reinhorn AM, Shinozuka M, Tierney K, Wallace WA, Von Winterfeldt D. A framework to quantitatively assess and enhance the seismic resilience of communities. Earthquake Spectra 2003; 19(4): 733-752. https://doi.org/10.1193/1.1623497

[40] Punetha P, Shanmugam GK. Experimental Evaluation of Encased Stone Column Technique for Liquefaction Mitigation. Proceedings of GeoShanghai 2018 International Conference: Advances in Soil Dynamics and Foundation Engineering, Singapore 2018.

[41] Shansuo Z, Zhigang S, Jinchuan H, Hao Z, Jinqi D. Method and application of economic loss assessment for earthquake disasters. Journal of Catastrophology 2020; 35(01): 94-101. https://doi.org/10.3969/j.issn.1000-811X.2020.01.018

[42] Cimellaro GP, Reinhorn AM, Bruneau M. Framework for analytical quantification of disaster resilience. Eng Struct 2010; 32(11): 3639-3649. https://doi.org/10.1016/j.engstruct.2010.08.008

[43] Cimellaro GP, Malavisi M, Mahin S. Factor Analysis to Evaluate Hospital Resilience. ASCE-ASME J Risk Uncertainty Eng Syst Part A Civ Eng 2018; 4(1): 04018002. https://doi.org/10.1061/AJRUA6.0000952

[44] Zhong S, Clark M, Hou X-Y, Zang Y, FitzGerald G. Validation of a framework for measuring hospital disaster resilience using factor analysis. Int J Environ Res Public Health 2014; pp. 6335-6353. https://doi.org/10.3390/ijerph110606335

https://doi.org/10.65904/3083-3590.2026.02.03